Current Biology 23, 2140–2145, November 4, 2013 ©2013 Elsevier Ltd All rights reserved http://dx.doi.org/10.1016/j.cub.2013.08.054

Report

Quantitative Imaging of Transcription in Living *Drosophila* Embryos Links Polymerase Activity to Patterning

Hernan G. Garcia,[1] Mikhail Tikhonov,[1,2] Albert Lin,[1] and Thomas Gregor[1,2,*]
[1]Joseph Henry Laboratories of Physics, Princeton University, Princeton, NJ 08544, USA
[2]Lewis-Sigler Institute for Integrative Genomics, Princeton University, Princeton, NJ 08544, USA

Summary

Spatiotemporal patterns of gene expression are fundamental to every developmental program. The resulting *macroscopic* domains have been mainly characterized by their levels of gene products [1–3]. However, the establishment of such patterns results from differences in the dynamics of *microscopic* events in individual cells such as transcription. It is unclear how these microscopic decisions lead to macroscopic patterns, as measurements in fixed tissue cannot access the underlying transcriptional dynamics [4–7]. In vivo transcriptional dynamics have long been approached in single-celled organisms [8–12], but never in a multicellular developmental context. Here, we directly address how boundaries of gene expression emerge in the *Drosophila* embryo by measuring the absolute number of actively transcribing polymerases in real time in individual nuclei. Specifically, we show that the formation of a boundary cannot be quantitatively explained by the rate of mRNA production in each cell, but instead requires amplification of the dynamic range of the expression boundary. This amplification is accomplished by nuclei randomly adopting active or inactive states of transcription, leading to a collective effect where the fraction of active nuclei is modulated in space. Thus, developmental patterns are not just the consequence of reproducible transcriptional dynamics in individual nuclei, but are the result of averaging expression over space and time.

Results

To monitor the transcriptional dynamics that lead to the formation of these boundaries, we have adapted a technique from single-celled organisms [8–12] that has been previously used to track mRNA in fly embryos [13]. Our technique allows for in vivo monitoring of nascent mRNA transcripts using a DNA sequence that upon transcription forms an mRNA stem loop. Cassettes with multiple copies of the stem loop are bound specifically by a constitutively expressed protein fused to GFP resulting in spatially localized fluorescence (Figure 1A).

Using this technique, we examine the step-like expression of the Bicoid (Bcd) activated *hunchback* (*hb*) P2 enhancer and promoter (Figures S1A and S1B available online), one of the best-studied expression patterns in the fly embryo [14, 15]. The P2 enhancer is one of three enhancers involved in the establishment of the endogenous *hb* pattern [16]. Reporter constructs for the P2 enhancer constitute an easily accessible model for the formation of developmental patterns in general, rather than reflecting on endogenous pattern formation. We drive the expression of a *lacZ* reporter gene with the mRNA stem loops located at its 5′ end (Figure 1A). Approximately 5 min into the ninth round of nuclear division, nuclear cycle (n.c.) 9, fluorescent spots associated with nuclei emerge within the syncytial blastoderm (Figure 1B). We detect single peaks of fluorescence activity during well-defined time windows that are synchronous with the rapid nuclear cycles in the early embryo (Movie S1). In n.c. 14, the expected step in zygotic expression is apparent in a surface layer of cells along the ~500 μm long axis of the embryo (Figure 1C). The bright spots are sites of nascent transcript formation, as confirmed by mRNA fluorescence in situ hybridization (FISH) [17]. Their fluorescence is directly proportional to the number of actively transcribing polymerase molecules (Figures S2A and S2B). Thus, we extract fluorescent traces reflecting transcriptional activity in individual nuclei as a function of space and time (Figures 1D and S2C–S2G).

To validate that these fluorescence dynamics faithfully recapitulate actual transcription, we measure the rate of transcript elongation in live embryos. This is accomplished by using an additional reporter construct in which the MS2 stem loops are located at the 3′ end of the *lacZ* gene, instead of the 5′ end. Upon entering a n.c., the onset of expression of the 3′ construct shows a clear delay with respect to the 5′ one (Figure 2A and Movie S2). The time delay measured over multiple embryos yields a rate of elongation $r_{elongation}$ = 1.54 ± 0.14 kb/min (Figure 2A). Measurements performed in *Drosophila* cell culture and in fixed embryos of 1.1–1.5 kb/min [18] are in agreement with our approach, suggesting that our technique gives direct access to the underlying transcriptional dynamics.

To connect the dynamics of transcription initiation (5′ signal) to the dynamics of transcription termination (3′ signal), we compare the fluorescent traces obtained with the two constructs in n.c. 14 (Figure 2B). Given the difference in construct geometry (see the Supplemental Experimental Procedures) and the same rate of polymerase loading, the overall signal of the 5′ construct should contain 3.6 times more labeled mRNA molecules than the 3′ construct. A deviation from 3.6 would indicate that not all initiated mRNA molecules are terminated and are possibly aborted during elongation. We find a ratio between the maximum polymerase loading of both signals of 3.3 ± 0.5, consistent with the majority of mRNA molecules being transcribed to termination. Therefore the dynamics of the larger 5′ signal can be used as a proxy for the production of full transcripts.

We link the transcriptional dynamics of the 5′ construct to the emergence of the macroscopic pattern, whose formation results from the accumulation of cytoplasmic mRNA transcripts with a half-life of over 3 hr [19] (in comparison, endogenous *hb* transcripts are stable for ~60 min [17]). This accumulation of mRNA is estimated by integration of the fluorescence traces of individual transcription spots over time (Figure S3A). We recover the spatial profile by averaging these integrated traces over nuclei in bins of 2.5% egg length (EL) along the anterior-posterior (AP) axis (Figures 3A, S3A, and

*Correspondence: tg2@princeton.edu

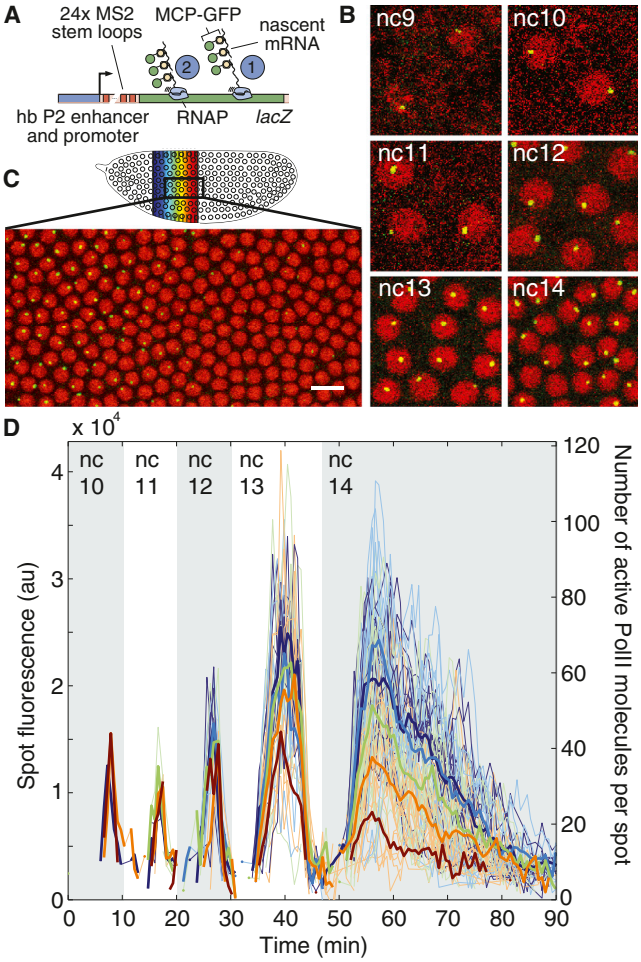

Figure 1. In Vivo Tracking of Transcriptional Activity using mRNA Stem Loops

(A) The *hb* P2 enhancer controlling the *hb* P2 promoter transcribes a *lacZ* gene with 24 MS2 stem loops located at its 5′ end. The MCP-GFP protein that binds to the stem loops is provided maternally.

(B) Snapshots (26 × 26 μm^2) of the anterior region of an embryo expressing the MS2-MCP system in nuclear cycles 9 through 14, showing MCP-GFP (green) and Histone-RFP (red) fluorescence. Brightness and contrast of each time point were adjusted independently.

(C) Typical field of view of an embryo between 30%–50% egg length (EL), anterior facing left. The scale bar represents 10 μm. See also Movie S1.

(D) Fluorescence traces corresponding to individual spots of transcription (thin lines) color-coded by their nuclear position along the embryo as shown in (B) and corresponding mean fluorescence over position-binned nuclei (thick lines).

See also Figure S1 and Movie S1.

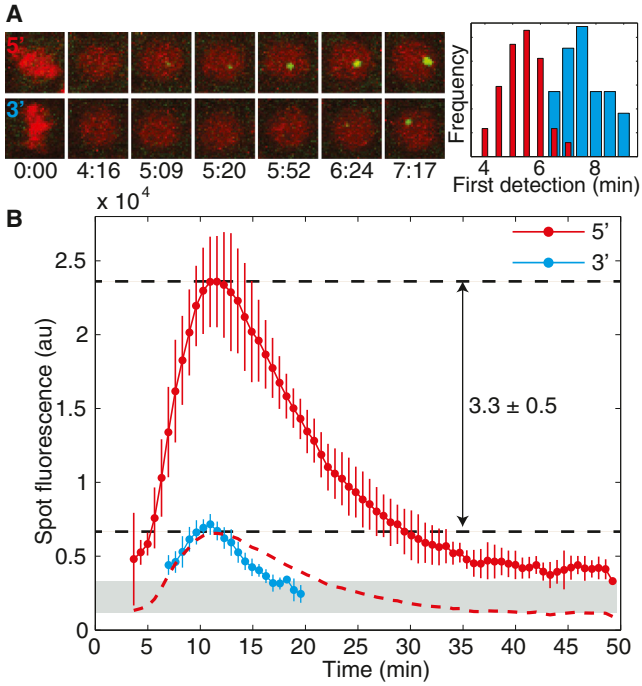

Figure 2. Rate of Transcript Elongation and Dynamics of Initiation and Termination

(A) Comparison of expression dynamics of a single allele of the enhancer-construct in two nuclei (different embryos) with stem loops located at the 5′ end and the 3′ end of the *lacZ* gene, respectively. Images (7 × 7 μm^2) show Histone-RFP (red) and MCP-GFP (green) fluorescence; time 0 min corresponds to anaphase 13. The histogram shows the distribution of times of first spot detection. The difference of the distribution means (i.e., 5.4 ± 0.1 min [red] and 7.6 ± 0.2 min [blue]) is used to measure the rate of transcript elongation $r_{elongation}$ = 1.54 ± 0.14 kb/min (difference between 5′ and 3′ stem loop locations is 3.4 kb; errors are propagated from the SE of the distributions; number of nuclei, $n_{5'}$ = 34 and $n_{3'}$ = 22).

(B) Average fluorescence in n.c. 14 as measured by the 5′ and 3′ constructs. The ratio between the maximum 5′ and 3′ fluorescence level is 3.3 ± 0.5, consistent with the predicted ratio of 3.6 based on gene length. The red dashed line is the 5′ signal rescaled by 3.6. The gray bar is the estimated detection limit of 6 ± 3 nascent mRNA molecules per spot (Figure S2H and Movie S2).

See also Figures S2 and S3 and Movie S2.

S3B). Comparison of this spatial profile to that obtained by FISH counts of cytoplasmic transcripts confirms that the patterns obtained with both methods are comparable within experimental error (Figures S3D–S3H).

mRNA FISH also provides a control for the behavior of our construct in terms of absolute counts of mRNA molecules. We count an absolute number of (220 ± 20) molecules produced per nucleus in the anterior region during n.c. 13 (Figures S3D–S3H). Assuming uniform polymerase loading on the gene and that each fluorescent spot contains two replicated sister chromatids [17, 20], this number corresponds to an average spacing of 150 ± 30 bp per gene, and a loading rate of one molecule every 6 ± 1 s per promoter. These results are consistent with absolute counts of endogenous *hb* mRNA and the maximum estimated rate of polymerase loading in fixed embryos [17, 21]. These numbers allow us to calibrate the integrated profile (Figure 3A) and the fluorescent traces (Figure 1D) in terms of the absolute number of mRNA molecules produced and the number of actively transcribing polymerase molecules, respectively (Figure S3H).

Developmental boundaries are characterized by the width of their transition region and their dynamic range of expression (Figure 3A and S1B). The width determines the spatial resolution of adjacent developmental states [3, 22], while a large dynamic range allows for deterministic downstream decisions [23, 24]. Our obtained spatial profile displays a first clear sign of a boundary during n.c. 13. The width of the transition does not change significantly between n.c. 13 (21% ± 2% EL) and n.c. 14 (20% ± 2% EL). On the other hand, the dynamic range of the boundary changes noticeably between n.c. 13 and n.c. 14 from 5.8 ± 0.8 to 26 ± 2 (Figure 3A), as confirmed by *lacZ*-mRNA FISH (Figure S3H).

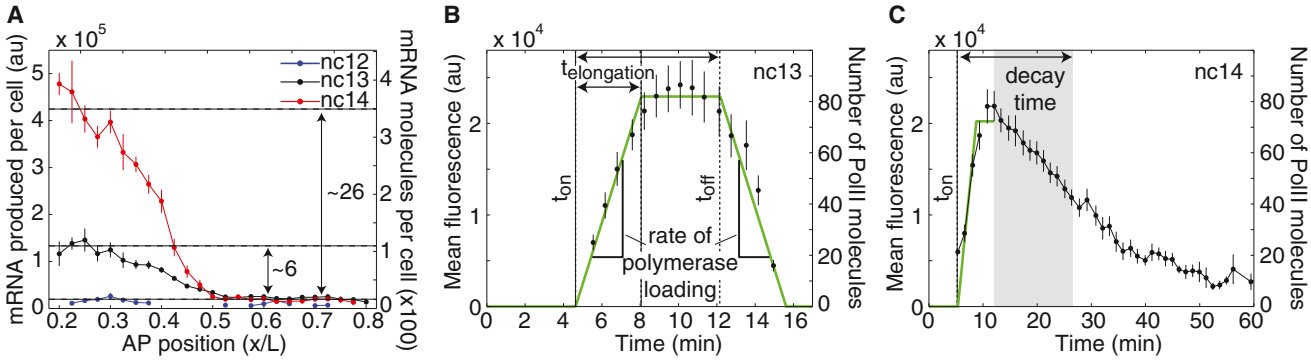

Figure 3. Dynamics of Boundary Formation

(A) Total amount of mRNA produced as a function of AP position for n.c. 12 (blue; n = 13), n.c. 13 (black; n = 24), and n.c. 14 (red; n = 24) (see the main text and Figures S3A–S3C). mRNA production is normalized per equivalent n.c. 14 cell (i.e., the production per cell in n.c.12 and n.c. 13 is divided by four and two, respectively); error bars show the SE over multiple embryos. The dynamic range, defined as the ratio between maximum and minimum expression of the pattern (Figure S1B), is 5.8 ± 0.8 and 26 ± 2 for n.c. 13 and n.c. 14, respectively.

(B and C) Model of transcriptional dynamics: transcription is turned on at a time t_{on} after mitosis with a constant rate of polymerase loading, resulting in a linear increase in fluorescence. After a time $t_{elongation}$ = 3.4 ± 0.3 min (i.e., the ratio between the length of the gene of 5.4kb and $r_{elongation}$), the first polymerase that was loaded will terminate transcription and leave the transcription site. A steady state of polymerase density (i.e., a stable fluorescence level) between newly loaded and terminating polymerases will persist until the promoter is turned off at t_{off}. Polymerase loading ceases, and the remaining polymerases terminate transcription at the reverse (negative) rate with which they were loaded. The difference between the turn off and turn on times defines the transcription time window (top arrows). The green curve shows a typical three-parameter fit to the mean fluorescence of nuclei located in a bin of size 2.5% EL centered around 30% EL in n.c. 13 (B) and n.c. 14 (C). In (C), only t_{on} and the rate of polymerase loading are determined by the fit; for determination of t_{off} in (C), see Figures S4A and S4B.

All errors show the SE over multiple nuclei. See also Figures S1 and S4.

Our live-imaging approach gives us the opportunity to determine the microscopic dynamics of transcription that lead to the formation of macroscopic pattern boundaries. The modulation of transcription along the AP axis is thought to determine the differential accumulation of gene product that ultimately generates the boundary (Figure S1B). Nuclei are expected to determine their rate of RNA polymerase (RNAP) loading based on the local concentration of the Bcd input gradient (Figures S1A and S1D) [2, 23, 25, 26]. Additionally, the window of time over which transcription occurs is modulated due to varying Bcd activator concentration during interphase (Figure S1C–S1E) [27]. In order to extract the rate of polymerase loading and the time window of active transcription at different positions along the AP axis, we use a simple effective model of transcription. In this model, the promoter becomes active at a time t_{on} after mitosis and RNAP molecules are loaded at a constant rate. This effective rate is the combination of microscopic processes such as polymerase binding to the promoter, promoter-proximal pausing and its subsequent release. At a time t_{off}, the promoter is turned off and polymerase loading ceases, defining the window of time (t_{off}–t_{on}) over which transcription is active (Figures 3B and 3C). We find that the proposed model closely follows the average time trace of all active transcription sites within a given 2.5% EL region during n.c. 13 (Figure 3B). The equivalent traces during n.c. 14 follow similar initial dynamics, but display a slowly decreasing fluorescence signal (Figures 3C, S4A, and S4B). It is plausible that in n.c. 13 transcription initiation is being turned off by the decay in nuclear Bcd levels upon mitosis entry [27] or by mitotic repression [28]. In contrast, transcription in n.c. 14 shuts down an hour before any cell undergoes mitosis. This shutdown could be related to the presence of high gap gene expression levels at that stage whose repressive function overrules that of the Bcd activator [27, 29, 30].

By fitting our model to the data, we extract the rate of polymerase loading and the time window of transcription as a function of AP position (Figures S4F and S4G). As expected from the pattern of mRNA accumulation (Figures 3A and S1), the rate of polymerase loading in individual nuclei is modulated along the AP axis in a step-like manner (Figure 4A). Nuclei in the anterior region express at higher rates than nuclei in the posterior region, and the levels both in n.c. 13 and n.c. 14 are comparable. The average rate of polymerase loading in the posterior of the embryo is given by the basal activity of the reporter construct in the absence of the Bcd activator (Figures 4A and S5 and Movie S3). In contrast to the rate of polymerase loading, the window of time during which transcription is active displays only a moderate variation along the AP axis during n.c. 12 and 13 (Figures 4B and S4C–S4E). However, n.c. 14 shows a clear modulation in the transcription time window as a function of AP position with a dynamic range of 1.9 ± 0.1.

Are these two extracted parameters (i.e., the effective *rate of polymerase loading* and the *transcription time window*) sufficient to recover the measured total amount of mRNA? In our effective model of transcription and in the absence of any other regulatory mechanisms, the total amount of mRNA produced per nucleus (Figure 3A) should equal the product of these two extracted parameters (Figures 4A and 4B). Indeed, we find a reasonable agreement between the two curves in n.c. 13 (Figure 4C, green and black curves), indicating that the modulation of these two microscopic parameters is enough to explain the formation of the macroscopic pattern. However, in n.c. 14 the same approach fails to quantitatively reproduce the directly measured total amount of mRNA (Figure 4D, green and red curves). Combining dynamic ranges of 4.8 ± 0.2 (rate of polymerase loading; Figure 4A) and 1.9 ± 0.1 (time window; Figure 4B) is not enough to recover the observed 26- ± 2-fold dynamic range in n.c. 14. Therefore, an additional regulatory mechanism that serves as an amplifier

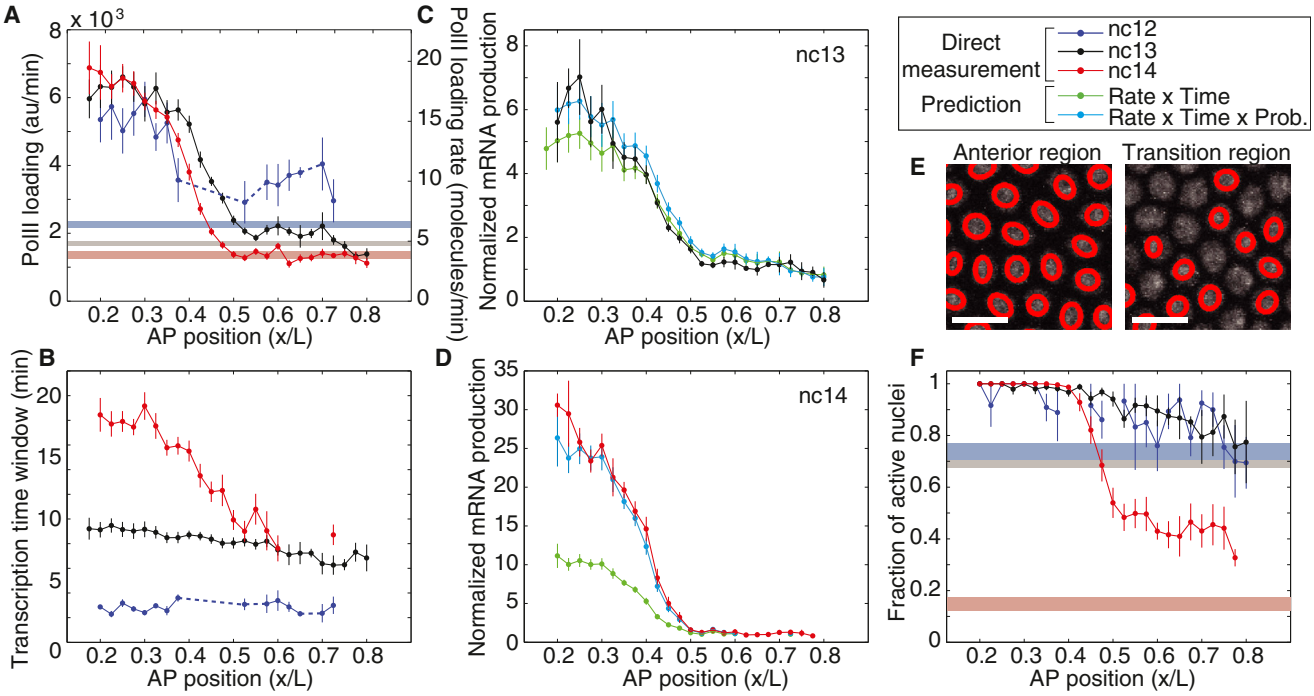

Figure 4. Formation of the Pattern Boundary Has Three Independent Dynamical Components

(A and B) Mean rate of polymerase loading (A) and mean window of time for transcription (B) as a function of position along the AP axis (for n.c. 12 [blue; n = 13 embryos], n.c. 13 [black; n = 24], and n.c. 14 [red; n = 24]; Figures S4A–S4E). Background values corresponding to a nonfunctional Bcd fly line are shown as horizontal bars using the same color coding (Figure S5 and Movie S3). See Figures S4F and S4G for a summary of transcription dynamics.

(C and D) mRNA produced as a function of AP position in n.c. 13 (C) and n.c. 14 (D). Data are normalized to the posterior end of the profiles. The direct measurement corresponds to the data shown in Figure 3A. Predictions (green and cyan) are obtained by multiplying the different values obtained in (A), (B), and (F).

(E) Representative fields of view (Histone-RFP) of nuclei in n.c. 14 in the activation (left, 29% EL) and transition regions (right, 61% EL). Nuclei where transcription was detected at any point over the entire n.c. are circled in red (Movies S4). Noncircled nuclei did not display any detectable transcription over the whole n.c. Scale bars represent 10 μm.

(F) Mean fraction of active nuclei as a function of position along the AP axis (Figure S6B). Color coding is as in (A) and (B).

In (A), (B), and (F), error bars show the SE over multiple embryos; in (C) and (D), error bars in the predictions are obtained by propagating the errors from (A), (B), and (F). See also Figures S5 and S6 and Movies S3 and S4.

for the dynamic range of the final gene expression boundary is necessary.

The mechanism of this amplifier is revealed by quantifying the number of nuclei in which transcription is detected as a function of AP position. All nuclei anterior to the boundary show expression, whereas only a fraction of the posteriorly located nuclei display activity (Figure 4E and Movie S4). No transcription is detected in inactive nuclei at any time point in the cycle. In n.c. 12 and 13, the local fraction of active nuclei across the boundary is only moderately modulated (Figure 4F). However, a strong modulation in the fraction of active nuclei is observed in n.c. 14, with a dynamic range of 2.3 ± 0.1. Interestingly, the fraction of active nuclei at the posterior end, where vanishing concentrations of Bcd protein are present [26], is higher than the fraction of active nuclei in the absence of Bcd (Figures 4F and S5D). This might indicate a uniform Bcd-dependent change in overall capacity of nuclei to transcribe. Moreover, we observe no preference for inactive n.c. 13 nuclei to divide into inactive daughter nuclei in n.c. 14, indicating that the state of nuclear activity is not transmitted through mitosis 13 (Figure S6A).

The switching of nuclei in n.c. 14 is independent of the control of the rate of polymerase loading. First, although the profile of the rate of polymerase loading is comparable in n.c. 13 and 14 (Figure 4A), the control of the fraction of active nuclei only becomes relevant in n.c. 14 (Figure 4F). This behavior indicates an overall change in transcription leading to the onset of the regulation of nuclear activity. Second, the rate of polymerase loading and the fraction of active nuclei present significantly different spatial patterns in n.c. 14 (Figure S6B), suggesting that they are distinct consequences of the input activator. Finally, lack of detection of active nuclei in n.c. 14 is not due to a substantial fraction of fluorescent spots falling below our detection limit. We estimate our systematic error to be less than 5%, well below the detected modulation in the fraction of active nuclei (Figure S2I).

Adding regulation of nuclear activity to our model leads to a good agreement between the directly measured total amount of mRNA produced and the product of the three dynamic parameters (Figure 4D, cyan and red curves), i.e., the *rate of polymerase loading*, the *transcription time window*, and the *fraction of active nuclei*. The random patches of active and inactive nuclei along the boundary (Figure 4E and Movie S4) eventually lead to a final smooth cytoplasmic mRNA profile (Figure S3H), suggesting that averaging at the level of cytoplasmic mRNA both in space and time is required [17, 23]. Therefore, it is these three basic microscopic features of transcriptional dynamics that are both necessary and sufficient to describe the formation of the macroscopic boundary.

Discussion

In multicellular organisms the formation of macroscopic patterns is believed to be the result of dynamical decisions made in individual cells [23, 31]. However, this relation cannot be tested using available fixed-tissue techniques, as they are unable to directly report on the dynamics of transcription. By monitoring transcriptional dynamics in living embryos we demonstrate that the formation of a pattern boundary can only be partially described by the modulation of the rate of polymerase loading and the time window of transcription (Figure 4D). The large dynamic range of developmental transcription boundaries is only recovered when the extra regulation of stochastic nuclear activity is added. Cytoplasmic mRNA patterns result from the average production of active nuclei over space and time. Such a regulatory strategy is not restricted to a syncytial blastoderm, where all nuclei share a common cytoplasm. In the presence of membranes, activated cells could still secrete signaling molecules in order to reach a similar spatiotemporal averaging of the output [32, 33].

Based on fixed tissue experiments, it has been suggested that the presence of nuclei with random activation states is related to various mechanisms of transcriptional precision [6, 7]. However, we were able to shed light on the role of this regulation in the formation of patterns in the early *Drosophila* embryo only through direct live imaging of nuclear activity. For example, it was unclear whether stochastic transcription corresponds to nuclei turning on and off repeatedly or whether it results from nuclei not turning on at all over the whole nuclear cycle. Here, we provide evidence for the latter scenario. Furthermore, this mechanism has no clear analog in single-cell systems, and its molecular basis remains unclear. The fact that it occurs only during n.c. 14, but not in any of the previous cycles, suggests that its onset may be related to the midblastula transition (MBT) [34]. MBT marks the large-scale activation of the zygotic genome resulting in the presence of additional factors such as gap genes and repressor gradients that can change the regulatory landscape [2, 35–37]. In fact, posterior repressor gradients have been suggested to play a key role in the establishment of boundaries and could be responsible for the observed stochastic inactivation of nuclear activity [37]. A systematic screen in mutant backgrounds will be required in order to uncover which molecular species is responsible for this stochastic regulation.

Our quantification of the dynamics of transcriptional regulation and of its relationship to pattern formation exemplifies the level of genetic and quantitative control available in the fly embryo. This approach can be extended to other reporter constructs and to endogenous genes in *Drosophila* and in other multicellular organisms. In particular, it will be interesting to determine how the dynamics of the wild-type *hb* boundary compares to the dynamics observed in the context of the simple construct addressed in this work.

Experimental Procedures

Female virgins maternally expressing MCP-GFP and Histone-RFP were crossed with males of the reporter line. Collected embryos were imaged using two-photon microscopy [26]. At each time point, a stack of ten images separated by 1 μm was acquired. MCP-GFP spots are detected and quantified in 3D [17] and assigned to the closest segmented nucleus. All animal usage is under the approval of Princeton University's Institutional Animal Care and Use Committee.

For details on transgenic fly construction, sample preparation, and data acquisition and analysis for both live imaging and mRNA FISH, please refer to the Supplemental Experimental Procedures.

Supplemental Information

Supplemental Information includes Supplemental Experimental Procedures, six figures, and four movies and can be found with this article online at http://dx.doi.org/10.1016/j.cub.2013.08.054.

Acknowledgments

We thank S. Blythe, E. Cox, S. Di Talia, L. Gavis, T. Idema, S. Little, R. Phillips, T. Schüpbach, A. Sgro, and E. Wieschaus for helpful discussions and comments on the manuscript. This work was supported by NIH grants P50 GM071508 and R01 GM097275, by a Princeton Dicke Fellowship (H.G.G.), and by Searle Scholar Award 10-SSP-274 (T.G.).

Received: July 26, 2013
Revised: August 23, 2013
Accepted: August 28, 2013
Published: October 17, 2013

References

1. Poustelnikova, E., Pisarev, A., Blagov, M., Samsonova, M., and Reinitz, J. (2004). A database for management of gene expression data in situ. Bioinformatics *20*, 2212–2221.
2. Jaeger, J., Surkova, S., Blagov, M., Janssens, H., Kosman, D., Kozlov, K.N., Manu, Myasnikova, E., Vanario-Alonso, C.E., Samsonova, M., et al. (2004). Dynamic control of positional information in the early Drosophila embryo. Nature *430*, 368–371.
3. Dubuis, J.O., Samanta, R., and Gregor, T. (2013). Accurate measurements of dynamics and reproducibility in small genetic networks. Mol. Syst. Biol. *9*, 639.
4. Paré, A., Lemons, D., Kosman, D., Beaver, W., Freund, Y., and McGinnis, W. (2009). Visualization of individual Scr mRNAs during Drosophila embryogenesis yields evidence for transcriptional bursting. Curr. Biol. *19*, 2037–2042.
5. McHale, P., Mizutani, C.M., Kosman, D., MacKay, D.L., Belu, M., Hermann, A., McGinnis, W., Bier, E., and Hwa, T. (2011). Gene length may contribute to graded transcriptional responses in the Drosophila embryo. Dev. Biol. *360*, 230–240.
6. Perry, M.W., Boettiger, A.N., and Levine, M. (2011). Multiple enhancers ensure precision of gap gene-expression patterns in the Drosophila embryo. Proc. Natl. Acad. Sci. USA *108*, 13570–13575.
7. Lagha, M., Bothma, J.P., Esposito, E., Ng, S., Stefanik, L., Tsui, C., Johnston, J., Chen, K., Gilmour, D.S., Zeitlinger, J., and Levine, M.S. (2013). Paused Pol II coordinates tissue morphogenesis in the Drosophila embryo. Cell *153*, 976–987.
8. Bertrand, E., Chartrand, P., Schaefer, M., Shenoy, S.M., Singer, R.H., and Long, R.M. (1998). Localization of ASH1 mRNA particles in living yeast. Mol. Cell *2*, 437–445.
9. Golding, I., Paulsson, J., Zawilski, S.M., and Cox, E.C. (2005). Real-time kinetics of gene activity in individual bacteria. Cell *123*, 1025–1036.
10. Yunger, S., Rosenfeld, L., Garini, Y., and Shav-Tal, Y. (2010). Single-allele analysis of transcription kinetics in living mammalian cells. Nat. Methods *7*, 631–633.
11. Larson, D.R., Zenklusen, D., Wu, B., Chao, J.A., and Singer, R.H. (2011). Real-time observation of transcription initiation and elongation on an endogenous yeast gene. Science *332*, 475–478.
12. Lionnet, T., Czaplinski, K., Darzacq, X., Shav-Tal, Y., Wells, A.L., Chao, J.A., Park, H.Y., de Turris, V., Lopez-Jones, M., and Singer, R.H. (2011). A transgenic mouse for in vivo detection of endogenous labeled mRNA. Nat. Methods *8*, 165–170.
13. Forrest, K.M., and Gavis, E.R. (2003). Live imaging of endogenous RNA reveals a diffusion and entrapment mechanism for nanos mRNA localization in Drosophila. Curr. Biol. *13*, 1159–1168.
14. Driever, W., and Nüsslein-Volhard, C. (1989). The bicoid protein is a positive regulator of hunchback transcription in the early Drosophila embryo. Nature *337*, 138–143.
15. Margolis, J.S., Borowsky, M.L., Steingrímsson, E., Shim, C.W., Lengyel, J.A., and Posakony, J.W. (1995). Posterior stripe expression of

hunchback is driven from two promoters by a common enhancer element. Development *121*, 3067–3077.
16. Perry, M.W., Bothma, J.P., Luu, R.D., and Levine, M. (2012). Precision of hunchback expression in the Drosophila embryo. Curr. Biol. *22*, 2247–2252.
17. Little, S.C., Tikhonov, M., and Gregor, T. (2013). Precise developmental gene expression arises from globally stochastic transcriptional activity. Cell *154*, 789–800.
18. Ardehali, M.B., and Lis, J.T. (2009). Tracking rates of transcription and splicing in vivo. Nat. Struct. Mol. Biol. *16*, 1123–1124.
19. Thomsen, S., Anders, S., Janga, S.C., Huber, W., and Alonso, C.R. (2010). Genome-wide analysis of mRNA decay patterns during early Drosophila development. Genome Biol. *11*, R93.
20. Shermoen, A.W., McCleland, M.L., and O'Farrell, P.H. (2010). Developmental control of late replication and S phase length. Curr. Biol. *20*, 2067–2077.
21. O'Brien, T., and Lis, J.T. (1991). RNA polymerase II pauses at the 5′ end of the transcriptionally induced Drosophila hsp70 gene. Mol. Cell. Biol. *11*, 5285–5290.
22. Crauk, O., and Dostatni, N. (2005). Bicoid determines sharp and precise target gene expression in the Drosophila embryo. Curr. Biol. *15*, 1888–1898.
23. Gregor, T., Tank, D.W., Wieschaus, E.F., and Bialek, W. (2007). Probing the limits to positional information. Cell *130*, 153–164.
24. Yu, D., and Small, S. (2008). Precise registration of gene expression boundaries by a repressive morphogen in Drosophila. Curr. Biol. *18*, 868–876.
25. Rosenfeld, N., Young, J.W., Alon, U., Swain, P.S., and Elowitz, M.B. (2005). Gene regulation at the single-cell level. Science *307*, 1962–1965.
26. Liu, F., Morrison, A.H., and Gregor, T. (2013). Dynamic interpretation of maternal inputs by the Drosophila segmentation gene network. Proc. Natl. Acad. Sci. USA *110*, 6724–6729.
27. Gregor, T., Wieschaus, E.F., McGregor, A.P., Bialek, W., and Tank, D.W. (2007). Stability and nuclear dynamics of the bicoid morphogen gradient. Cell *130*, 141–152.
28. Shermoen, A.W., and O'Farrell, P.H. (1991). Progression of the cell cycle through mitosis leads to abortion of nascent transcripts. Cell *67*, 303–310.
29. Jaeger, J. (2011). The gap gene network. Cell. Mol. Life Sci. *68*, 243–274.
30. Liu, J., and Ma, J. (2013). Uncovering a dynamic feature of the transcriptional regulatory network for anterior-posterior patterning in the Drosophila embryo. PLoS ONE *8*, e62641.
31. Davidson, E.H. (2006). The Regulatory Genome: Gene Regulatory Networks in Development and Evolution (Burlington: Academic Press).
32. Lewis, J. (2008). From signals to patterns: space, time, and mathematics in developmental biology. Science *322*, 399–403.
33. Lander, A.D. (2013). How cells know where they are. Science *339*, 923–927.
34. Tadros, W., and Lipshitz, H.D. (2009). The maternal-to-zygotic transition: a play in two acts. Development *136*, 3033–3042.
35. Ahmad, K., and Henikoff, S. (2001). Modulation of a transcription factor counteracts heterochromatic gene silencing in Drosophila. Cell *104*, 839–847.
36. Bai, L., Ondracka, A., and Cross, F.R. (2011). Multiple sequence-specific factors generate the nucleosome-depleted region on CLN2 promoter. Mol. Cell *42*, 465–476.
37. Chen, H., Xu, Z., Mei, C., Yu, D., and Small, S. (2012). A system of repressor gradients spatially organizes the boundaries of Bicoid-dependent target genes. Cell *149*, 618–629.

Current Biology, Volume *23*

Supplemental Information

Quantitative Imaging of Transcription in Living *Drosophila* Embryos Links Polymerase Activity to Patterning

Hernan G. Garcia, Mikhail Tikhonov, Albert Lin, and Thomas Gregor

SUPPLEMENTAL EXPERIMENTAL PROCEDURES

Cloning of transgenes

A pUC18 vector containing the construct pNOS-NLS-MCP-eGFP-αTub3'UTR was kindly provided by Liz Gavis (Princeton University). This construct contains the MS2 coat protein (MCP) fused to eGFP under the control of the *nanos* promoter. It bears a nuclear localization signal (NLS) and an αTubulin 3'UTR. The NLS was removed by amplifying the plasmid with primers 2.14 and 2.15. The resulting plasmid pUC18-pNOS-NLS-MCP-eGFP-αTub3'UTR was then inserted into pCASPER4 using the KpnI and HpaI sites for P-element transgenesis. NLS-MCP-GFP has been reported to localize in puncta within nuclei even in the absence of reporter in the early embryo [S1]. This artifact could be completely abolished by removing the nuclear localization signal from MCP-GFP while still maintaining significant protein levels within nuclei. 12 copies of the stem loops were extracted from plasmid pSL-MS2-12X (Addgene 27119) by digesting with PsiI and EcoRV. This fragment was ligated back into pSL-MS2-12X digested with EcoRV in order to create pSL-MS2-24X. Plasmid piB-hbP2-P2P-lacZ- αTub3'UTR was kindly provided by Steve Small (NYU) [S2]. It contains the *hunchback* P2 enhancer and promoter driving the *lacZ* gene fused to an αTubulin 3'UTR. This sequence is flanked by attB sites, which can be used for recombinase-mediated cassette exchange (RMCE) into the fly genome at specific landing sites [S3]. In order to insert the MS2 stem loops into this reporter construct unique restriction sites were created either at the 5' or 3' of the *lacZ* gene using site-directed mutagenesis (Quikchange II; Stratagene). For the 5' construct NcoI and AvrII sites were created using primer 1.12. This plasmid was digested using the two new restriction enzymes and combined with an NcoI-AvrII fragment from pSL-MS2-24X in order to create piB-hbP2-P2P-MS2-24x-lacZ-αTub3'UTR.

Primer name and number	Sequence	Description
2.14-Pnos-NoNLS-CCW	tattatatgcatgatctatggaaaatccgggtcg	Amplify the pUC18-pNOS-NLS-MCP-eGFP-αTub3'UTR plasmid while deleting the NLS and inserting an NsiI site
2.15-Pnos-NoNLS-CW	attataatgcatcaccatggcttctaactttactcagttcgtt	
1.12-P2PupV2-NcoI-NsiI	cgtctagagccgccaagtacccatggctatcacaatgcatatgcagaactgggagacgac	Create NcoI and AvrII sites at the 5' end of the *lacZ* gene in piB-hbP2-P2P-lacZ- αTub3'UTR
1.5-P2PlacZdw-NcoI-NsiI	gtctggtgtcaaaaataaccatggctatcacaatgcattaataaccgggcagg	Create NcoI and NsiI sites at the 3' end of the *lacZ* gene in piB-hbP2-P2P-lacZ- αTub3'UTR

For the 3' construct, NcoI and NsiI sites were created using primer 1.5. Here, the plasmid was digested with the new restriction sites and ligated with a fragment obtained from pSL-MS2-24X using the same restriction enzymes in order to create piB-hbP2-P2P-lacZ-MS2-24x-αTub3'UTR. The resulting geometry of our reporter constructs is such that polymerases in the 5' construct transcribe through the 1336bp long MS2 region and through 3960bp more DNA until reaching the end of the transcript, while in the 3' construct transcription continues only through 605bp after the loops. All steps were confirmed by sequencing. Plasmids and plasmid sequences are available upon request.

Fly strains and genetics

The construct pCASPER4-pNOS-MCP-eGFP-αTub3'UTR was randomly inserted into the fly genome using P-element transgenesis (BestGene). Several clones were isolated. For this particular work, a line on the III chromosome, called *MCP-NoNLS(2)*, was established. A *Histone-RFP* fusion (*His2Av-mRFP1,* FBti0077845) on the second chromosome was used to create the fly line *yw*;*Histone-RFP*;*MCP-NoNLS(2)*. Line *Bcd-GFP*;*Histone-RFP*;Bcd^{E1} for the measurements shown in Figure S1C was generated from lines *Bcd-GFP*;Bcd^{E1} [S4] and *Histone-RFP*. To determine the activity of our

reporter in the absence of Bcd activator the *Bcd^{E1}* and *MCP-GFP* lines were recombined to create *yw*;*Histone-RFP*;*Bcd^{E1},MCP-NoNLS(2)*. Constructs piB-hbP2-P2P-MS2-24x-lacZ-αTub3'UT and piB-hbP2-P2P-lacZ-MS2-24x-αTub3'UTR were inserted into the fly genome using the RMCE approach [S3] to create fly lines *P2P-MS2-lacZ* and *P2P-lacZ-MS2*, respectively.

Sample preparation and data acquisition

Female virgins of line *yw;Histone-RFP;MCP-NoNLS(2)* or of *yw*;*Histone-RFP*;*Bcd^{E1},MCP-NoNLS(2)* were crossed with males of the reporter line (*P2P-MS2-lacZ* or *P2P-lacZ-MS2*). Collected embryos were dechorinated and mounted between a semipermeable membrane (Biofolie, In Vitro Systems & Services) and a coverslip and embedded in Halocarbon 27 oil (Sigma). Excess oil was removed with absorbent paper from the sides in order to flatten the embryos slightly. The flattening of the embryos makes it possible to image more nuclei in the same focal plane without causing any detectable change to early development processes [S5]. Embryos were imaged using a custom-built two-photon microscope [S6] with a laser wavelength of 970 nm to excite both MCP-GFP and Histone-RFP. Fluorescence was collected with two separate photomultiplier tubes (gallium-arsenide-phosphide photomultiplier tube, module H10770PA-40 SEL Hamamatsu). Pixel size is 220 nm and image resolutions are 512x256 pixels or 128x128 pixels. At each time point a stack of 10 images separated by 1 μm was acquired. For each slice of the stack three individual images were taken, aligned and averaged offline. The final time resolution is 37s (512x256 window) and 10s (128x128 window), respectively.

Live imaging data analysis

Histone-RFP slices were maximum projected for each time point. Nuclei were segmented using available segmentation software optimized for *Drosophila* early embryonic development [S7]. The segmented nuclei were then tracked over multiple nuclear cycles by adapting an available code [S8]. Initially, each time frame of the MCP-GFP channel is treated independently. Spots are detected in 3D using raw images [S9, 10] (Figure S2I) and assigned to their respectively closest nucleus. When multiple spots are detected in the vicinity of the nucleus (due to segregating sister chromatids) only the brightest one is kept. When single traces are shown, the automated tracking of both nuclei and spots was checked manually frame by frame using custom analysis code. Spot intensity determination requires an estimate of the local fluorescent background for each particle. 2D Gaussian fits to the peak plane of each particle column (Figure S2I) determines an offset, which is used as background estimator. The intensity is calculated by integrating the particle fluorescence over a circle with a radius of 6 pixels and subtracting the estimated background. Imaging error is dominated by the error made in the fluorescent background estimation (Figure S2C-G).

Single molecule mRNA FISH sample preparation and data analysis

Single molecule mRNA FISH was performed as previously described [S9, 10]. Probes against the *lacZ* gene were functionalized with Atto565 dye. To avoid degradation of endogenous GFP fluorescence, methanol washed and incubations in the FISH protocol [S9, 10] were sped up as much as possible. Data was analyzed as described in [S9].

SUPPLEMENTAL FIGURES

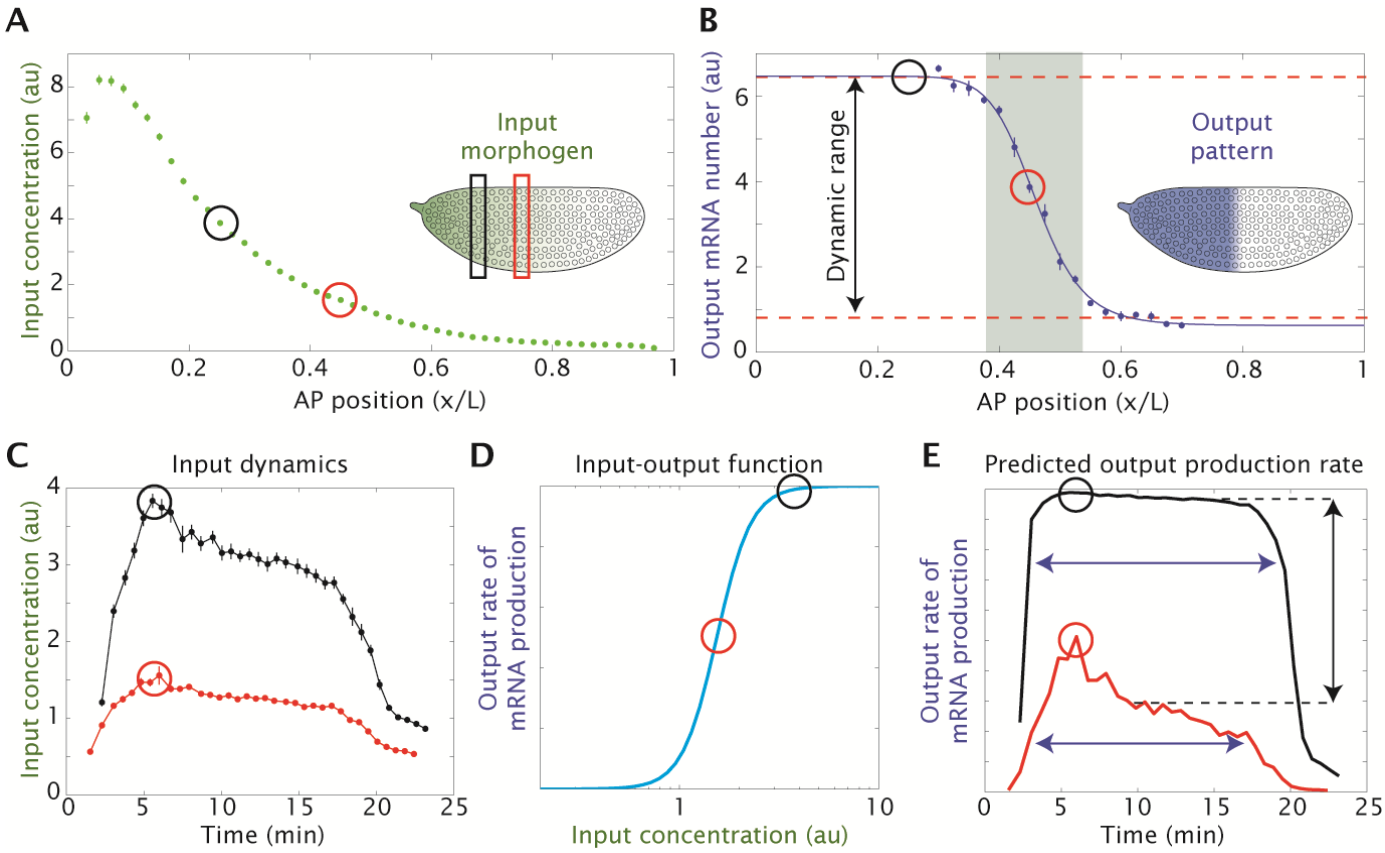

Figure S1. Dynamic developmental pattern formation, related to Figures 1 and 3. **(A-B)** A space-varying input morphogen (A, data shown for Bcd-GFP [S6]) determines an output pattern of accumulation of its target gene (B, measured by counting accumulated transcripts). The dynamic range and transition region (shaded area) of the boundary are shown. Black and red circles indicate measurements in nuclei in the anterior and in the transition regions of the profile throughout the figure, respectively. **(C)** The nuclear concentration of the Bcd input morphogen is subject to spatial modulation as in (A) and, in addition, to temporal modulation throughout the nuclear cycle (colors indicate nuclear averages at two positions in the embryo (see (A)). **(D)** An input-output function has been hypothesized to determine the output *rate of mRNA production* as a function of the instantaneous input concentration of transcription factor [S11-14]. **(E)** The input-output function in (D) coupled with the input dynamics in (C) predicts the modulation of the average rate of mRNA production of the output gene (black arrow) and of the window of time over which transcription ensues (blue arrows). (A, error bars are standard errors over multiple embryos; B,C, error bars are standard errors over multiple nuclei).

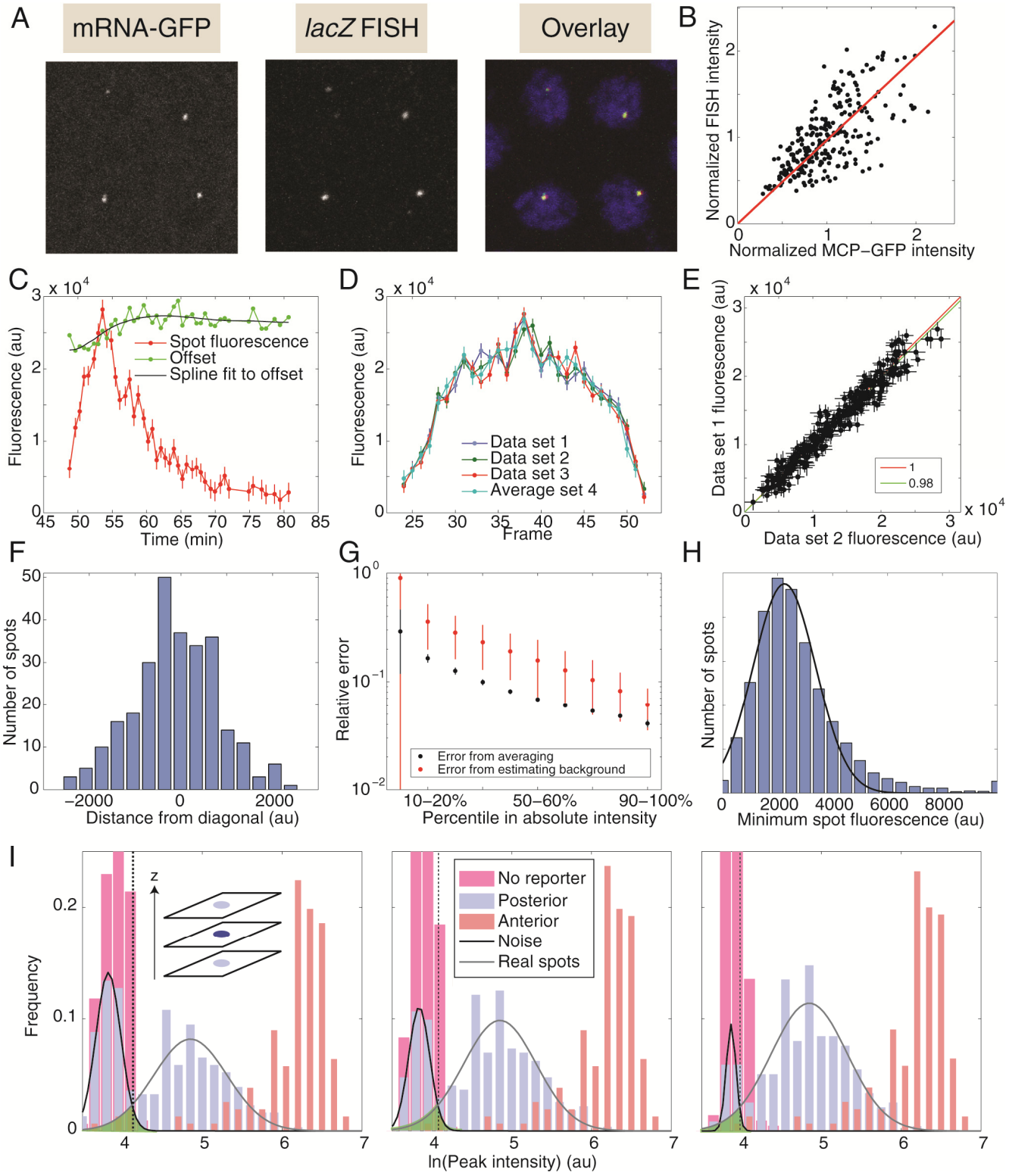

Figure S2. Spot detection and fluorescence measurement, related to Figure 2. (A) MCP-GFP spots are related to sites of nascent transcripts. Embryos were fixed during interphases 13 and 14 and stained using oligonucleotide probes against *lacZ* mRNA. Fluorescent spots in the *lacZ* FISH channel have been previously shown to be sites of nascent transcripts [S9, 15]. A strong co-localization between these spots and spots of preserved endogenous GFP expression in the MCP-GFP channel is observed (larger than 90%, n=2). Images are 15μm x 15μm. Extra spots in the *lacZ* FISH channel correspond to finished individual mRNA transcripts that cannot be resolved in the MS2 channel or to sites of nascent transcription with a load of

RNAP below the detection limit. Overlay shows MCP-GFP (green), *lacZ* FISH (red) and DAPI (blue) channels. **(B)** The spot intensities in the MCP-GFP channel correlate with the corresponding intensities of nascent transcription spots in the FISH channel, which had previously been shown to be a measure of the number of actively transcribing PolII molecules [S9]. Intensities in both channels are normalized to their means. Red line is a linear fit with zero y-intercept. The large spread of the data is a signature of the stochastic RNAP distributions along the gene. FISH probes are distributed along the length of the mRNA, and therefore their intensities report on the total length of nascent mRNA at a site of transcription. Polymerases will appear brighter the closer they are to 3' end of the transcript. A given number of polymerases can therefore give rise to a range of possible intensities. **(C, left inset)** A Difference-of-Gaussian (DoG) filter is applied to all planes imaged at a given time point [S9, 10]. This filter maximizes the contrast in each image. Spots found in at least three consecutive planes are combined into a column. Spots that cannot fulfill this requirement are rejected. A second selection occurs by thresholding on the DoG value of the shadow plane. The third selection corresponds to only assigning one spot per nucleus. When multiple spots are found in the vicinity of a nucleus the brightest one is kept. Finally, the resulting distribution of DoG values in the peak plane is explored. **(C)** Typical spot trace and fluorescent offset signal as a function of time in the anterior region in n.c. 14. A 2D Gaussian fit to each particle at every time point is performed in order to estimate the fluorescent background (green). The resulting background as a function of time is fitted to a spline (black line). Spot intensity is calculated by integrating the particle fluorescence over a circle with a radius of 6 pixels and subtracting the background estimated from the spline at each time point (red). The standard deviation of the offset of the data around this spline is used to determine the imaging error associated with each particle. The errors in offset and particle fluorescence measurements are assumed to be comparable and uncorrelated. Hence the error in spot fluorescence is approximated by the offset error times $\sqrt{2}$. **(D-G)** To estimate the imaging noise, fluorescent traces are taken at a frame rate four times higher than our standard protocol while maintaining the same exposure and assembled into four different data sets of the same embryo. **(D)** Fluorescence as a function of frame number for the same spot as measured using the different data set sets shows that the traces are comparable. **(E)** Fluorescence of each spot at each time point in data set 1 as a function of the corresponding fluorescence in data set 2. Red line has a slope of one and green line is a linear fit with a slope of 0.98. This fit is performed for all combinations of data sets to obtain an average slope of 0.99±0.01 (mean±SD). No noticeable correlation between the spread of the data around the line and the intensity is observed. **(F)** Histogram of distance to the fitted line of each data point in (D). The average root-mean-square (RMS) distance with respect to the fitted line for the data set combinations is $(1.0\pm0.1)\times10^3$ arbitrary fluorescence units (au) (mean±SD). **(G)** Relative error in fluorescence intensity as a function of the spot intensity. The absolute spot intensities are sorted into different percentiles and the error stemming from averaging (black) and from estimating the offset (red, see(D)) is computed. Error bars are standard deviations. From this plot we conclude that the uncertainty in determining the offset is higher than the uncertainty stemming from averaging multiple frames. When individual spot traces are plotted the error in estimating the background is used as a proxy for the total error in estimating the fluorescence. **(H)** Histogram of the minimum fluorescence per detected particle for all collected data ($n_{particles}\approx5800$). Black line is a fit to a normal distribution to estimate a detection limit, which can be converted using the absolute calibration (Figure S3) to 6±3 nascent mRNA molecules per fluorescent spot. **(I)** Systematic error associated with detecting dim spots in the posterior region of the boundary is determined by selecting the brightest peak plane DoG values observed throughout the life of each nucleus and plotting them in a histogram. The different plots indicate choices of the threshold applied on the shadow plane (32.5, 35 and 37.5 from left to right). Blue bars correspond to data taken in the posterior region, where the overall transcription signal is low. Red bars correspond to data taken in the anterior region. Magenta bars stem from data taken in the absence of the reporter construct. The left peak found in the distribution of posterior spots (blue) is associated with noise which can contribute to our count as false positives. This is justified by the fact that the left peak coincides with the control distribution obtained in the absence of reporter. The right peak of the blue distribution corresponds to real spots. In the case of the anterior distribution all spots detected are real spots due to the fact that every nucleus is turned on. As a result, no noise peak is noticeable in the histogram. In order to estimate the percentage of false positives and false negatives two Gaussians are fitted to the posterior distribution for different values of the shadow threshold. In each case the optimum threshold is determined by the intersection of the two Gaussian curves (dashed line located at 61.6, 58.9 and 41.6, respectively). The area under the Gaussian to the right of the threshold is used to estimate the fraction of false positives, and the fraction of false negatives is estimated from the area under the Gaussian to the left of the threshold (green shaded area) resulting in a systematic error for each threshold used of 5%, 4% and 10% from left to right. The clear separation between detected spots and noise fluorescence indicates that nuclei in which no spots are detected present no transcription or transcribe at levels that are significantly lower than our detection limit.

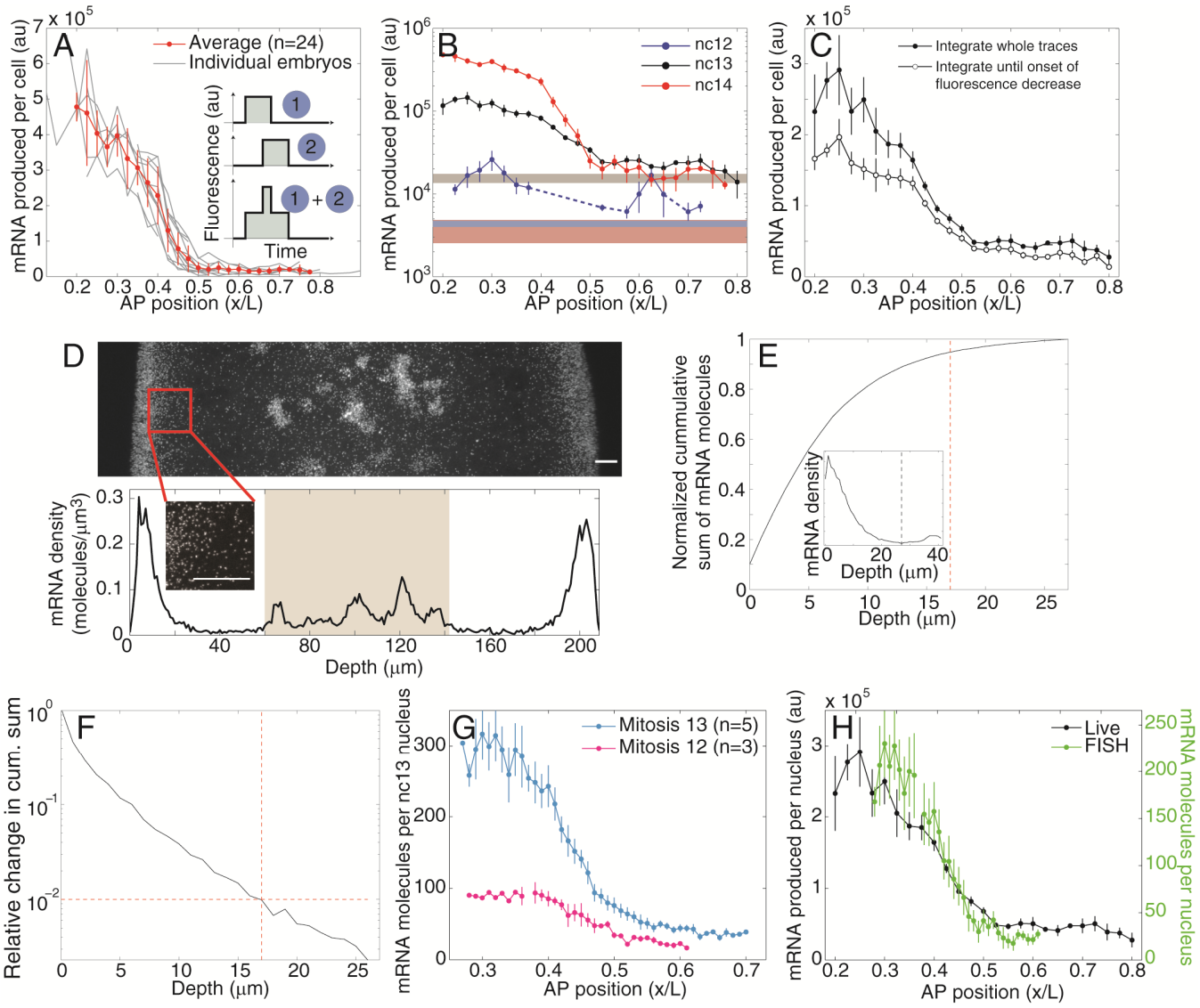

Figure S3. Inferring the absolute number of mRNA molecules accumulated, related to Figure 2. **(A)** (Inset: Each polymerase numbered as in Figure 1A will contribute to the overall fluorescence trace in an independent manner. The area under the fluorescence curve will be proportional to the total number of mRNA molecules produced). 24 profiles of the amount of mRNA produced as a function of AP (grey lines). Imaging window in individual embryos cover an AP range of ~20%EL. Full AP profile is obtained by averaging these profiles in 2.5%EL bins (red points). **(B)** Total amount of mRNA produced per n.c. 14-equivalent-cell (i.e. the production per cell in n.c.12 and n.c. 13 is divided by four and two, respectively, to compensate for nuclei associated cytoplasmic volume changes from n.c. to n.c.) as a function of AP position as in Figure 3A (note log scale on y-axis). Blue, gray and red horizontal bars correspond to the mean and standard error of the effective mRNA production in embryos carrying a *bcd*^{E1} mutation (Figure S5). **(C)** It is possible that not all PolII molecules contributing to the fluorescence result in a finished transcript. As a result, the calculation of the total amount of mRNA produced from the integral of fluorescent traces (Figure 3A) could be systematically overestimated. In particular, if the decrease in signal at the onset of fluorescent decay is due to mitotic repression [S16, 17], for example, none of the fluorescence past this time point should be considered. The systematic error in the integration is estimated by identifying the onset of mitotic repression with the promoter turn off time, t_{off} (Figure 3B). The overall number of mRNA molecules produced as a function of AP position shows a decrease with respect to integrating over the whole life of a spot of (29±9)%. However, the dynamic range remains comparable with 5.8±0.4 when integrating over the whole life time of spots and 5.8±0.8 when only considering their traces until t_{off}. We conclude that the dynamic range is not sensitive to the window of time of integration. On the other hand, the absolute value obtained from integration is sensitive to the time window, setting a bound on the reliability of the comparison of absolute levels measured by live imaging and mRNA FISH. **(D)** Typical midsagittal section in the anterior region of an embryo (~35%EL location along the AP axis) carrying a version of our reporter construct without the MS2 stem loops (top). Individual cytoplasmic mRNA molecules are resolved (inset) [S9]. The distribution of mRNA molecules peaks at the surface of the embryo and decays towards the interior yolk region (bottom). At a position midway to the center of the embryo the production from yolk nuclei

(peaks between 60μm and 140μm, shaded area) is significant. Due to embryo deformation stemming from the protocol these distances vary from embryo to embryo. Therefore, the optimum depth in the apical-basal direction for counting all cytoplasmic transcripts was determined independently for each embryo. Scale bar is 10μm. **(E)** Cumulative cytoplasmic *lacZ*-mRNA distribution integrated from the embryo surface to the optimum depth as a function of apical-basal depth. Inset shows the distribution of mRNA molecules as a function of depth into the embryo from which the optimal depth is determined (dashed black line). **(F)** The relative change in the cumulative sum as a function of depth, used to find a depth at which the sum changes by less than 1% (red dashed lines). This distance corresponds to more than 90% of all mRNA molecules detected (red dashed line in (D)). **(G)** Cytoplasmic mRNA profiles during mitosis 12 and 13 (averages of n=3 and n=5 embryos, respectively) when mRNA production is shut down [S16, 17]. Given the stability of the 3'UTR of our reporter construct [S18] we interpret these profiles as indicating the total amount of accumulated mRNA until mitosis 12 and 13, respectively. **(H)** The total amount of mRNA produced during n.c. 13 is obtained by subtracting the profile for mitosis 12 from the profile for mitosis 13 reported in (D). The obtained FISH profile is overlaid with the total amount of mRNA produced in n.c. 13 inferred from the MS2 data by normalizing to the anterior region. This provides a calibration of the live profile with absolute mRNA counts, allowing for reports of the absolute amount of produced mRNA (Figure 3A). Since the systematic error in measuring absolute levels with the live imaging technique can be as high as 29% this calibration should only be viewed as an estimate. Using this result we determine the integrated fluorescence intensity corresponding to the transit of one polymerase molecule along the gene (A, inset). Dividing this intensity value by the time of elongation (Figure 3B) yields an average fluorescence per polymerase molecule. Consequently, we calibrate the fluorescent traces in terms of the absolute number of transcribing polymerases per fluorescent spot (Figures 1D and 3B,C). The dynamic range of the two profiles is comparable (FISH 7.3±0.7 and MS2 5.8±0.8). The systematically wider transition region obtained from live imaging is attributed to the fact that the profile is constructed by averaging multiple embryos spanning only 20%EL as opposed to mRNA FISH which allows for the imaging of the whole profile in single embryos. (C, error bars are standard deviations over multiple embryos; D,E,G,H error bars are standard errors over multiple embryos).

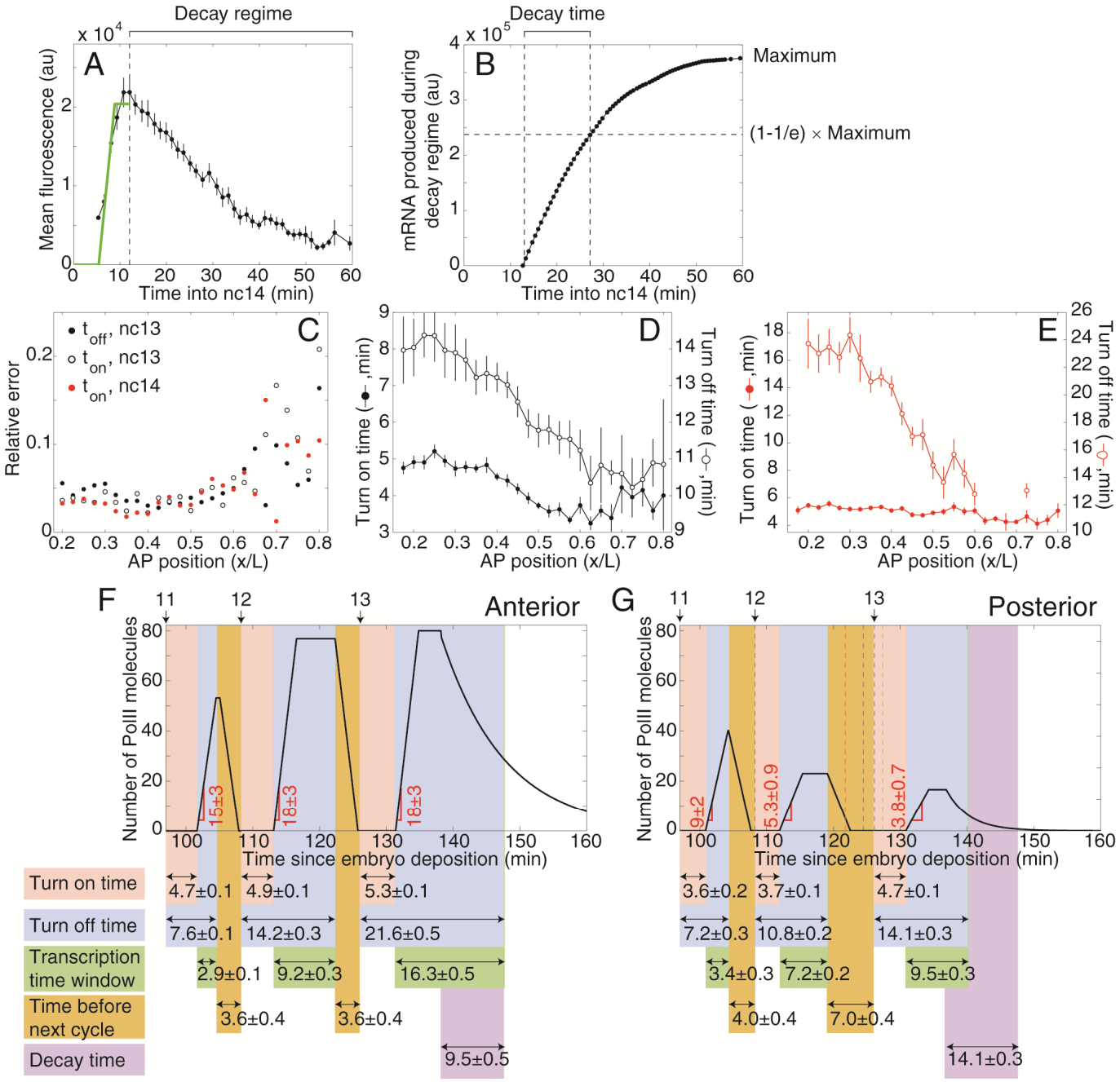

Figure S4. Extracting transcriptional dynamics using a simple model of regulation, related to Figure 3. **(A)** In n.c. 14 the first part of mean fluorescence as a function of time is fit using a model as described in the text (Figure 3B,C). The decay regime in n.c. 14 is defined from the point where the fluorescence starts decreasing (black dashed line) until the end of the trace (at 60 min). **(B)** The integral of the fluorescence in the decay regime corresponds to the amount of mRNA produced as a function of time (Figure S3A-C). The decay time is calculated by finding the time point at which the integrated signal is within 1/e of its maximum. This time is then used to calculate the time of transcription turn off, t_{off}. **(C)** As we move from anterior to posterior the detected spots have a smaller overall fluorescence, making it more difficult to discern them. As a result, the estimation of the time of promoter turn on and turn off will be affected. The plot shows the relative error of measurements of these turn-on and turn-off times as obtained by the fit to our model (Figure 3A,B) as a function of AP. For positions near the posterior end of the embryo the error in time determination can be as high as 20%. This error is small compared to the modulation of the time window in n.c. 14 of 1.9±0.1 (Figure 4B). **(D,E)** Time of promoter turn on (solid circles) and turn off (open circles) in n.c. 13 **(D)** and n.c. 14 **(E)** as a function of position along the embryo. Both the promoter turn on and turn off times are modulated in n.c. 13. However, they do so by keeping their difference almost constant resulting in a small

modulation of the window of time of active transcription (Figure 4B). In n.c. 14 only the time of promoter turn off displays a strong a modulation along the AP axis.**(F,G)** For n.c. 12, 13 and 14 the rate of polymerase loading (RNAP molecules/min, shown in red) and the different times related to the transcription process (in min) per fluorescent spot are shown for the (F) anterior and (G) regions. We define the beginning of a n.c. as the onset of anaphase. Transcription begins approximately 5 min into a n.c. and ends 3.6 min before the next n.c. Although interphases 12 and 13 last about 10 and 13 min, respectively [S19], the time during which polymerase loading occurs in the anterior region is only (2.9±0.1) min for n.c. 12 and (9.2±0.3) min for n.c. 13. (All errors are standard errors of the mean).

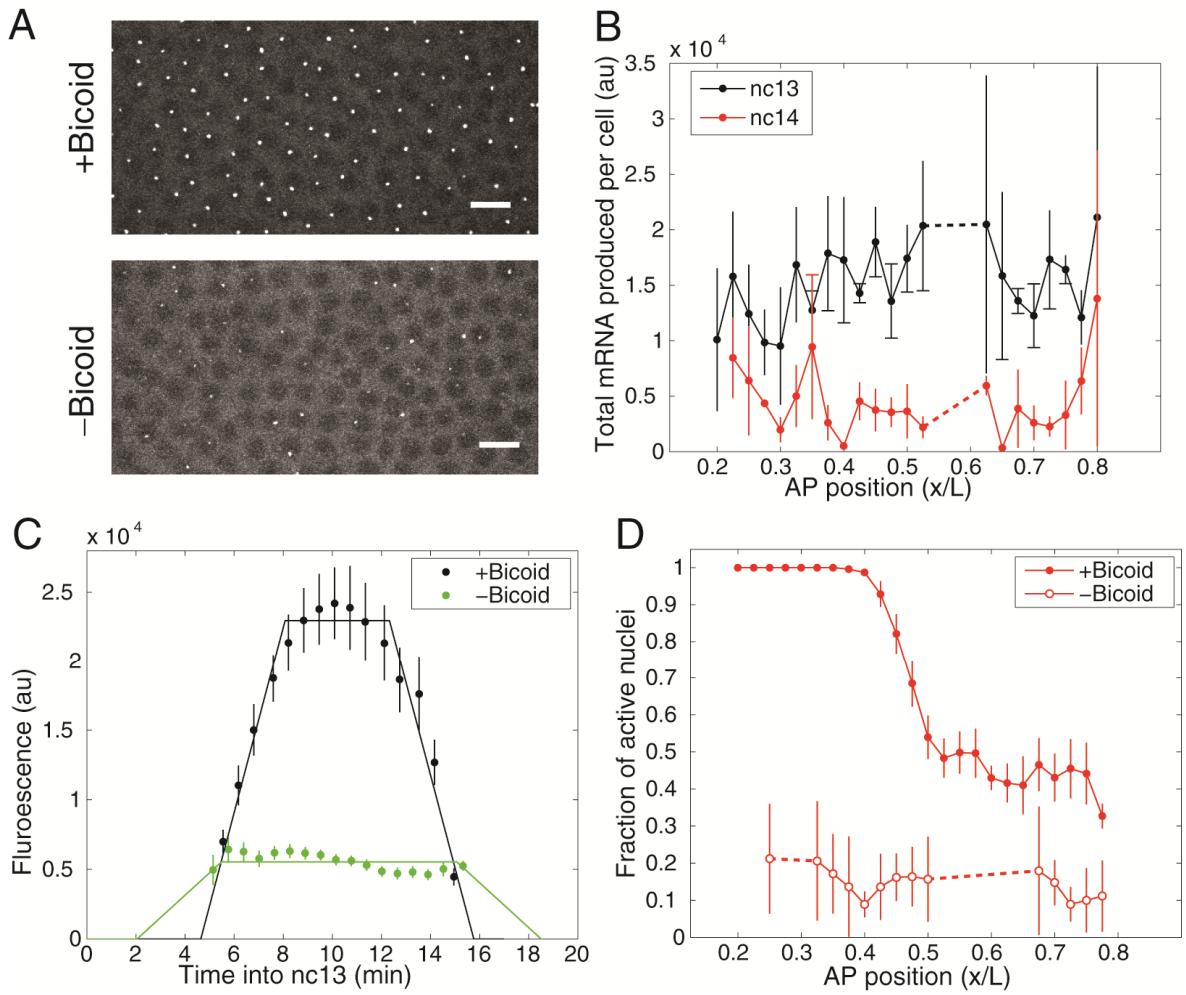

Figure S5. Basal transcriptional activity in the absence of Bcd, related to Figure 4. Throughout the embryo transcription sites are observed in the absence of the activator Bcd. **(A)** Comparison of a field of view in the anterior region in the presence (left) and absence (right) of Bcd activator in n.c. 13 (using the null mutant bcd^{E1}). Note that the brightness and contrast has been adjusted to make the presence of spots clear. Scale bar is 10 μm. **(B)** Total mRNA produced per n.c. 14 cell (i.e. the production per cell in n.c. 13 is divided by two) in the absence of Bcd for n.c. 13 (black) and n.c. 14 (red). The profiles show no clear dependence with AP position. The basal amount of mRNA produced by bcd^{E1} embryos is an order of magnitude lower than the amount produced in the anterior region in the presence of Bcd. **(C)** Average fluorescence of spots in wild-type (Ore-R) embryos (black, at 30% EL) and in bcd^{E1} mutant embryos (green, over the whole embryo) in n.c.13. The rate of transcription initiation of the bcd^{E1} mutant is obtained by fitting to our model (Figures 2B and 3B). **(D)** Fraction of active nuclei as a function of AP position in n.c. 14 in the presence of Bcd and in a bcd^{E1} mutant. Interestingly, the fraction of active nuclei at the posterior end, where vanishing concentrations of Bcd protein are present [S6], is 43±2%. However, in the absence of Bcd this number decreases to 15±2%, indicating a uniform Bcd-dependent change in overall capacity of nuclei to transcribe. We speculate on two possible molecular scenarios to explain this observation. First, the reporter construct could read out nuclear Bcd concentration in a non-equilibrium manner such that vanishing Bcd concentrations are distinguishable from not having Bcd at all. Second, a molecular species could be activated by a Bicoid-dependent process in the anterior region and diffuse throughout the embryo by n.c. 14, affecting the nuclear transcriptional capacity. (A, D, error bars are standard errors over multiple embryos; B, error bars are standard errors over multiple nuclei).

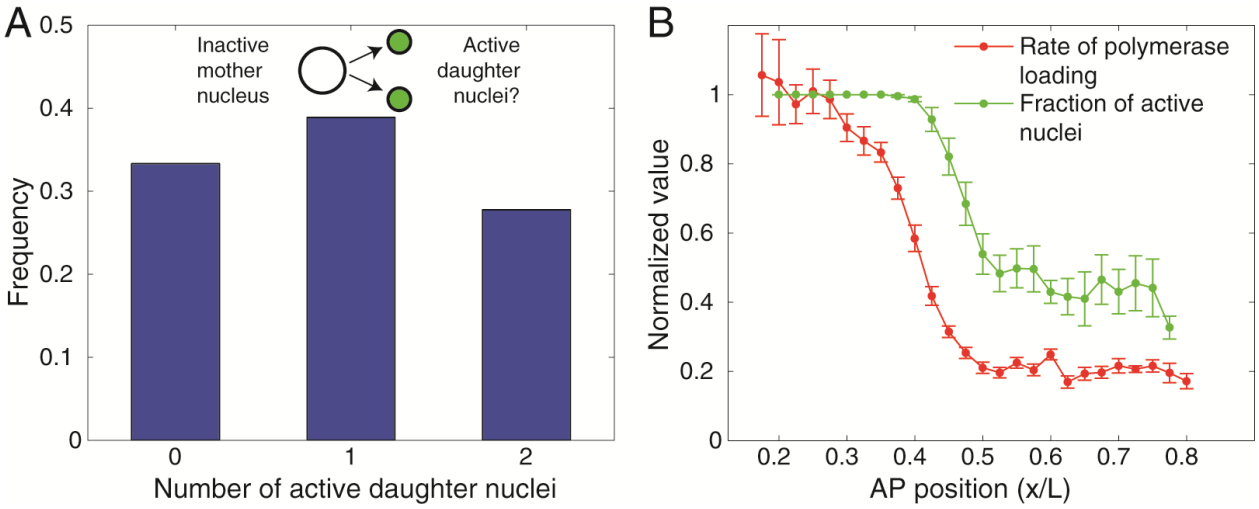

Figure S6. Control of the fraction of active nuclei, related to Figure 4. (**A**) Histogram of the number of active n.c. 14 daughter nuclei stemming from mother nuclei that were inactive (n=18). Nuclei that are inactive in n.c. 13 divide into daughter nuclei with no particular preference for activation in n.c. 14. This result suggests that the activity of a nucleus is stochastic and that the state of nuclear activity is not memorized. This observation contrasts with previous reports of a memory effect in the synchrony of early *hb* expression [S20]. (**B**) Rate of polymerase loading (red) and fraction of active nuclei (green) as a function of AP position. Data points are average and standard error over multiple embryos in AP bins of 2.5%. When arbitrarily normalizing the anterior region to 1 a clear boundary shift is detected. As a consequence, as one moves along the boundary from the anterior toward the posterior the rate of polymerase loading decreases while all nuclei are still active. Only when the rate of polymerase loading has decreased to ~50% of its peak value the modulation of the fraction of active nuclei becomes apparent. The fact that the two boundaries are not coinciding indicates that the two regulatory parameters are controlled in an independent fashion. As both parameters are Bcd dependent, it also indicates that the modulation of the fraction of activated nuclei is controlled by a loading-rate-independent interaction of Bcd with the P2 enhancer. This scenario can be realized if the rate of polymerase loading and the fraction of active nuclei are controlled by two different sets of binding sites on the P2 enhancer, each with a different dissociation constant. For instance, high affinity binding sites for Bcd could regulate chromatin accessibility, while lower affinity ones the rate of polymerase loading [S21, 22].

Supplemental References

S1. van Gemert, A.M., van der Laan, A.M., Pilgram, G.S., Fradkin, L.G., Noordermeer, J.N., Tanke, H.J., and Jost, C.R. (2009). In vivo monitoring of mRNA movement in Drosophila body wall muscle cells reveals the presence of myofiber domains. PLoS ONE *4*, e6663.

S2. Chen, H., Xu, Z., Mei, C., Yu, D., and Small, S. (2012). A system of repressor gradients spatially organizes the boundaries of bicoid-dependent target genes. Cell *149*, 618-629.

S3. Bateman, J.R., Lee, A.M., and Wu, C.T. (2006). Site-specific transformation of Drosophila via phiC31 integrase-mediated cassette exchange. Genetics *173*, 769-777.

S4. Gregor, T., Wieschaus, E.F., McGregor, A.P., Bialek, W., and Tank, D.W. (2007). Stability and nuclear dynamics of the bicoid morphogen gradient. Cell *130*, 141-152.

S5. Di Talia, S., and Wieschaus, E.F. (2012). Short-term integration of Cdc25 dynamics controls mitotic entry during Drosophila gastrulation. Developmental cell *22*, 763-774.

S6. Liu, F., Morrison, A.H., and Gregor, T. (2013). Dynamic interpretation of maternal inputs by the Drosophila segmentation gene network. Proc Natl Acad Sci U S A *110*, 6724-6729.

S7. Idema, T. (2013). A new way of tracking motion, shape, and divisions. European biophysics journal : EBJ.

S8. Young, J.W., Locke, J.C., Altinok, A., Rosenfeld, N., Bacarian, T., Swain, P.S., Mjolsness, E., and Elowitz, M.B. (2012). Measuring single-cell gene expression dynamics in bacteria using fluorescence time-lapse microscopy. Nat Protoc *7*, 80-88.

S9. Little, S.C., Tikhonov, M., and Gregor, T. (2013). Precise developmental gene expression arises from globally stochastic transcriptional activity. Cell *in press*.

S10. Little, S.C., Tkacik, G., Kneeland, T.B., Wieschaus, E.F., and Gregor, T. (2011). The formation of the Bicoid morphogen gradient requires protein movement from anteriorly localized mRNA. PLoS Biol *9*, e1000596.

S11. Rosenfeld, N., Young, J.W., Alon, U., Swain, P.S., and Elowitz, M.B. (2005). Gene regulation at the single-cell level. Science *307*, 1962-1965.

S12. Kuhlman, T., Zhang, Z., Saier Jr., M.H., and Hwa, T. (2007). Combinatorial transcriptional control of the lactose operon of \emph{Escherichia coli}. Proc Natl Acad Sci U S A *104*, 6043-6048.

S13. Bintu, L., Buchler, N.E., Garcia, H.G., Gerland, U., Hwa, T., Kondev, J., Kuhlman, T., and Phillips, R. (2005). Transcriptional regulation by the numbers: applications. Curr Opin Genet Dev *15*, 125-135.

S14. Jaeger, J., Surkova, S., Blagov, M., Janssens, H., Kosman, D., Kozlov, K.N., Manu, Myasnikova, E., Vanario-Alonso, C.E., Samsonova, M., et al. (2004). Dynamic control of positional information in the early Drosophila embryo. Nature *430*, 368-371.

S15. Wilkie, G.S., Shermoen, A.W., O'Farrell, P.H., and Davis, I. (1999). Transcribed genes are localized according to chromosomal position within polarized Drosophila embryonic nuclei. Curr Biol *9*, 1263-1266.

S16. Shermoen, A.W., and O'Farrell, P.H. (1991). Progression of the cell cycle through mitosis leads to abortion of nascent transcripts. Cell *67*, 303-310.

S17. Rothe, M., Pehl, M., Taubert, H., and Jackle, H. (1992). Loss of gene function through rapid mitotic cycles in the Drosophila embryo. Nature *359*, 156-159.

S18. Thomsen, S., Anders, S., Janga, S.C., Huber, W., and Alonso, C.R. (2010). Genome-wide analysis of mRNA decay patterns during early Drosophila development. Genome Biol *11*, R93.

S19. Foe, V.E., Odell, G.M., and Edgar, B.E. (1993). Mitosis and morphogenesis in the *Dropsophila* embryo: Point and counterpoint. In The Development of Drosophila melanogaster, M. Bate and A. Martinez Arias, eds. (Plainview, N.Y.: Cold Spring Harbor Laboratory Press).

S20. Porcher, A., Abu-Arish, A., Huart, S., Roelens, B., Fradin, C., and Dostatni, N. (2010). The time to measure positional information: maternal hunchback is required for the synchrony of the Bicoid transcriptional response at the onset of zygotic transcription. Development *137*, 2795-2804.

S21. Mirny, L.A. (2010). Nucleosome-mediated cooperativity between transcription factors. Proc Natl Acad Sci U S A *107*, 22534-22539.

S22. Lam, F.H., Steger, D.J., and O'Shea, E.K. (2008). Chromatin decouples promoter threshold from dynamic range. Nature *453*, 246-250.